RSC Advances

PAPER

View Article Online
View Journal | View Issue

Check for updates

Cite this: *RSC Adv.*, 2024, **14**, 38335

Study of the zeolite-catalyzed isomerization of 1-methylnaphthalene†

Shiyong Xing,‡*[a] Yan Cui,‡[bc] Fenglin Zhang,[a] Jianbin Su,[a] Kan Xu,[a] Xiaofei Liu,[b] Ziheng Chen,[b] Yuehua Zhao[b] and Minghan Han*[b]

Received 13th August 2024
Accepted 24th October 2024

DOI: 10.1039/d4ra05881j

rsc.li/rsc-advances

Isomerization of 1-methylnaphthalene (1-MN) to 2-methylnaphthalene (2-MN) is a crucial step in the production of 2,6-dimethylnaphthalene (2,6-DMN), which is an important raw material for polyethylene naphthalate (PEN). Herein, the isomerization of 1-MN was systemically investigated over beta zeolite. Firstly, reaction conditions were systemically optimized, by which enhanced catalytic performance was obtained. Thereafter, the effect of nitride on the catalytic performance was investigated using a series of characterization techniques and DFT calculations, revealing that firm adsorption of nitride on acid sites was the main reason for catalyst deactivation. Activity of the deactivated catalyst was difficult to recover *via* extraction with hot benzene. Fortunately, catalytic performance could be effectively recovered through coke-burning, wherein the framework and acid sites were well-preserved during calcination.

1. Introduction

During the past few decades, C10 aromatics have been mainly derived from ethylene cracking, catalytic reforming and high-temperature coal coking. Recently, the utilization of C10 aromatics has attracted increasing attention.[1–5] As a component of C10 aromatics, alkyl naphthalene accounts for about 40% of them, mainly including naphthalene, 1-MN, 2-MN, and dimethyl naphthalene isomers. Among these aromatics, 1-MN and 2-MN have been widely used in the petrochemical and fine chemical industries, such as synthetic fiber dyeing aids, surfactants, plasticizers, diffusing agents, and vitamin K3.[6–9] Recently, the preparation of 2,6-DMN *via* the alkylation of 2-MN with methanol or 2-MN transalkylation with polymethylbenzene has become a research hotspot.[1,2,5] Therefore, the industrial demand for 2-MN is much more than that for 1-MN, although 1-MN has its own applications, such as dyes.[6,10]

Research studies on the isomerization of 1-MN to 2-MN over zeolite catalysts have been widely reported. For example, Li *et al.* investigated the isomerization-transalkylation coupling reaction of 1-MN over zeolites with different topologies. They found that MWW, BEA and FAU zeolite with a 12-membered ring channel showed better catalytic activity compared with MFI zeolite with a 10-membered ring channel.[10] Sun *et al.* treated beta zeolite with oxalic acid and found that the selectivity of 2-MN was increased to 92.70% for the isomerization of 1-MN.[6] Generally, deactivation by coke is inevitable for zeolite-catalyzed reactions.[11–14] For the isomerization of 1-MN, Rombi *et al.* found that coke becomes more aromatic in nature with increasing reaction time, and its composition also changes with the same parameter. Popova *et al.* studied the isomerization of 1-MN over different zeolites, including Y, MOR, SAPO-5, and ZSM-5, and found that disproportionation proceeds to a lower degree, while the main reaction is isomerization.[15] Jens *et al.* found that zeolites with a spaciousness index between about 2 and 16 were more excellent in isomerization, and undesired disproportionation can be completely suppressed.[16]

As can be seen from previous investigations on the isomerization of 1-MN, solid acids account for a large part of the catalysts, which is mainly due to their eco-friendly characteristics. Among the solid acid catalysts, zeolites have attracted more attentions, mainly owning to their various frameworks, tunable acid properties, high thermal stability, regular channels with shape-selectivity, absence of corrosion and environmentally safe properties.[17–26]

In fact, C10 aromatics produced from the catalytic cracking of heavy oil usually contain some sulfide and nitride, which can cause severe air pollution when used as fuels.[27–30] Additionally, they can cause some negative effects on the downstream chemical processes. Therefore, desulfurization and denitrification are really important for petroleum processing.[31–35] For the isomerization of 1-MN, the effects of sulfide and nitride from C10 aromatics on the catalytic performance are still unknown, but worth investigating.

[a]*Beijing Special Engineering Design and Research Institute, Beijing 100028, China. E-mail: xingsy18@tsinghua.org.cn*

[b]*Beijing Key Laboratory of Green Chemical Reaction Engineering and Technology, Department of Chemical Engineering, Tsinghua University, Beijing 100084, P. R. China. E-mail: hanmh@tsinghua.edu.cn*

[c]*Petrochemical Research Institute, PetroChina Company Limited, Beijing 100195, China*

† Electronic supplementary information (ESI) available. See DOI: https://doi.org/10.1039/d4ra05881j

‡ Shiyong Xing and Yan Cui contributed equally to this work.

Open Access Article. Published on 03 December 2024. Downloaded on 2/11/2026 7:43:27 PM. This article is licensed under a Creative Commons Attribution-NonCommercial 3.0 Unported Licence.

Open Access Article. Published on 03 December 2024. Downloaded on 2/11/2026 7:43:27 PM. This article is licensed under a Creative Commons Attribution-NonCommercial 3.0 Unported Licence.

As a three-dimensional zeolite with a 12 member-ring large pore size, beta has been utilized in a variety of reactions. Especially for the reactions with large size molecules, the intersection of channels can provide important reaction spaces.[16,36–38] Additionally, the same level of size between products and channels can also improve the product selectivity. Therefore, beta zeolite was selected herein to give a comprehensive investigation on the isomerization of 1-MN. Firstly, a suitable reaction condition was determined by a series of catalyst evaluations. Then, the deactivation mechanism was comprehensively investigated by a series of characterization techniques and DFT calculations. Finally, the regeneration process was discussed in detail.

2. Methods

2.1 Experimental

2.1.1. Materials. 1-MN was provided by Petrochemical Research Institute, PetroChina Company Limited, and benzene (>99.5%) was purchased from the Beijing Tong Guang Fine Chemicals Company. All reagents were commercially received without further purification. Beta zeolite was synthesized according to the method describe in ref. 39. Other zeolites, *viz.*, MFI, EUO, MOR, MTW and FAU, were all provided by Petrochemical Research Institute, PetroChina Company Limited.

2.1.2. Catalytic evaluation. The isomerization of 1-MN was performed in a continuous-flow fixed bed micro-reactor (see Fig. S1†) at 4.2 MPa, consisting of a stainless tube reactor with a length of 50 cm and a diameter of 1 cm. A typical experiment was performed using 1 g catalyst mixed with 10 g quartz sand. Before the reaction, the catalyst was activated under 100 ml per min N_2 flow for 3 h at 300 °C. After cooling to the reaction temperature, benzene was firstly pumped into the reactor to reach 4.2 MPa. Then, the mixture of benzene and 1-MN with a certain weight percent was switched into the reactor. For the vapor phase reaction, the feedstocks should be accompanied with N_2 flow, and the reaction was conducted at 0.1 MPa. The effluent mixture was analyzed offline with a gas chromatograph (Shimadzu GC-14B) equipped with a flame ionization detector (FID). The catalyst was assumed to be deactivated as the conversion of 1-MN decreased below 60%, and then the lifetime was calculated. The deactivated beta using pure feedstocks were denoted as B-coke, while the deactivated zeolites using sulfide and nitride contaminated feedstocks were denoted as B-SN. It is worth noting that the concentration of 1-MN in the feedstocks is low, and the selectivity of 2-MN in the products is close to 100%. Therefore, this work mainly focused on the activity and stability.

2.1.3. Catalyst characterization. The crystalline structure of the samples was determined by Powder X-ray diffraction (XRD) using a Bruker D8 Advance powder X-ray diffractometer with Cu Kα radiation. The scanning range of 2θ was 2–50° at 2° min^{-1}. A physisorption analyzer (Quantachrome Autosorb iQ) was used to measure the surface areas and pore structure of the different samples at 77 K. For the morphology study, different samples were investigated by scanning electron microscopy (SEM) characterization conducted with a JSM7401 instrument. Transmission electron microscopy (TEM) images were recorded on a JEM2010 at 200 kV. Thermogravimetric analysis (TGA) and differential thermal analysis (DTA) experiments were performed on a TGA/DSC1/1600LF apparatus. The experiments were carried out in a temperature range of 25–800 °C under flowing air (100 ml min^{-1}), and with a heating rate of 10 °C min^{-1}. Ammonia temperature-programmed desorption (NH_3-TPD) was analyzed on a ChemBET Pulsar TPR/TPD. Typically, 0.1 g sample (40–60 mesh) was pretreated at 400 °C for 30 min under He flow (100 ml min^{-1}), and then cooled to 50 °C. After saturation with NH_3 for 45 min, He flow (100 ml min^{-1}) flushed the sample for 30 min to remove the weakly adsorbed NH_3 molecules. Then, the He flow (100 ml min^{-1}) was in contact with the sample with increasing temperature until 700 °C (ramp rate of 10 °C min^{-1}). ^{27}Al MAS NMR experiments were performed on a JNM-ECZ600R spectrometer at a resonance frequency of 156 MHz using a 4 mm double-resonance MAS probe at a sample spinning rate of 13 kHz. The chemical shift of ^{27}Al was referenced to 1 M aqueous $Al(NO_3)_3$. ^{27}Al MAS NMR spectra were recorded by small-flip angle technique using a pulse length of 0.4 μs (<π/15) and a recycle delay of 1 s. The amount of sulfide and nitride was determined by an A2070 analyzer.

2.2 Computational details

All periodic DFT calculations were performed using the Vienna *Ab initio* Simulation Package (VASP 5.3.5)[40,41] with the Grimme's D3 corrections[42] to describe the vdW interactions. The projector augmented wave (PAW) method[43,44] was used to describe the electron–ion interaction with the plane wave basis set kinetic energy cutoff of 400 eV. The Brillouin zone was sampled at the Γ point only by using the Monkhorst–Pack technique.[45] A force threshold of 0.02 eV $Å^{-1}$ was used for the geometry optimization of all intermediates.

The BEA cell was constructed according to the Structure Commission of the International Zeolite Association.[46] Firstly, the all-silicon form of the BEA cell was constructed in 1 × 1 × 1. The lattice constants were then optimized (12.66, 12.66, and

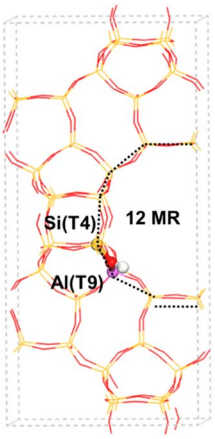

Framework	BEA
Formal composition	$Si_{64}O_{128}$
Acid site	Al(T9)-OH-Si(T4)
Ring sizes	12-ring
Pore size	6.6 × 6.7 Å
Si/Al ratio	63

Fig. 1 Geometry structures of H-BEA. Yellow: silicon; red: oxygen; purple: aluminum; white: hydrogen; gray: carbon. T represents the tetrahedral Si or Al atom. The same color scheme is used throughout the paper.

© 2024 The Author(s). Published by the Royal Society of Chemistry

Open Access Article. Published on 03 December 2024. Downloaded on 2/11/2026 7:43:27 PM.
This article is licensed under a Creative Commons Attribution-NonCommercial 3.0 Unported Licence.

26.58 Å) using an energy cutoff of 600 eV and a force threshold of 0.01 eV $Å^{-1}$. Considering the larger length of 1-dodecene, the 1 × 1 × 1 BEA cell will be extended when calculating the adsorption energy of 1-dodecene. For H-BEA, the substitution of the Si atom with the Al atom at T9 is energetically most favorable, as suggested by previous works.[47–50] The information of the optimized geometries of H-BEA is shown in Fig. 1.

The adsorption energy of guest species in zeolites was calculated as follows:

$$\Delta E_{ads} = E_{adsorbate/H\text{-}zeolite} - E_{adsorbate} - E_{H\text{-}zeolite} \quad (1)$$

The fundamental terms $E_{adsorbate/H\text{-}zeolite}$ and $E_{H\text{-}zeolite}$ are the energies of the zeolite cell with and without adsorbate, respectively, and $E_{adsorbate}$ is the energy of the isolated adsorbate.

3. Results and discussion

As can be seen from the previous publications, a variety of zeolites have been utilized in the isomerization of 1-MN.[6,10,51] Therefore, we firstly conducted this reaction over several zeolites with different frameworks, of which beta exhibited superior catalytic performance. The detailed information about the screening process can be found in the ESI (see Fig. S2).† Therefore, beta was selected herein to gain insight into the isomerization of 1-MN.

3.1 Characterization results

Firstly, the physical properties were characterized as follows. The morphology of beta can be characterized by TEM and SEM. As can be seen from Fig. 2a, the beta zeolite was aggregated with small crystals, and it is difficult to distinguish the crystals only from SEM images. Fortunately, the crystal size can be more clearly characterized by TEM. As can be seen from Fig. 2b, the crystal size is homogeneously distributed (~20 nm), although the crystals have irregular fringes. Fig. 2c shows the XRD patterns of beta zeolite. As can be seen, the diffraction peaks are in accordance with that of the previous publications, indicative of its pure phase.[37,52] The texture properties are shown in Fig. 2d and Table 1. As can be seen, the beta zeolite exhibits typical IV-type isothermals. The adsorption below 0.01 at the low-pressure range corresponds to the micropores. The adsorption step due to the capillary condensation at P/P_0 = 0.6–0.9 indicates the existence of mesopores, which originated from the aggregation of small crystals.

3.2 Catalytic performance

Firstly, the reaction conditions were comprehensively investigated. For the isomerization of 1-MN, different reaction phases have been reported previously, including vapor and liquid phase.[6,10,15,16] However, for the beta zeolite-catalyzed isomerization of 1-MN, the effect of the reaction phase on the catalytic performance has never been reported to the best of our knowledge. Therefore, the isomerization of 1-MN was firstly conducted on different phases as follows. As can be seen from Fig. 3, the conversion of 1-MN decreased rapidly after 3 h on the vapor phase, indicating its severe deactivation. However, the lifetime was prolonged to 9 h for the liquid phase. Therefore, it can be concluded that the liquid phase is more beneficial to the catalytic stability. The reaction on the liquid phase was further conducted once again to confirm this conclusion.

Based on the conclusions mentioned above, the following investigations were all performed on the liquid phase. The effect of the temperature, weight hourly space velocity (WHSV)

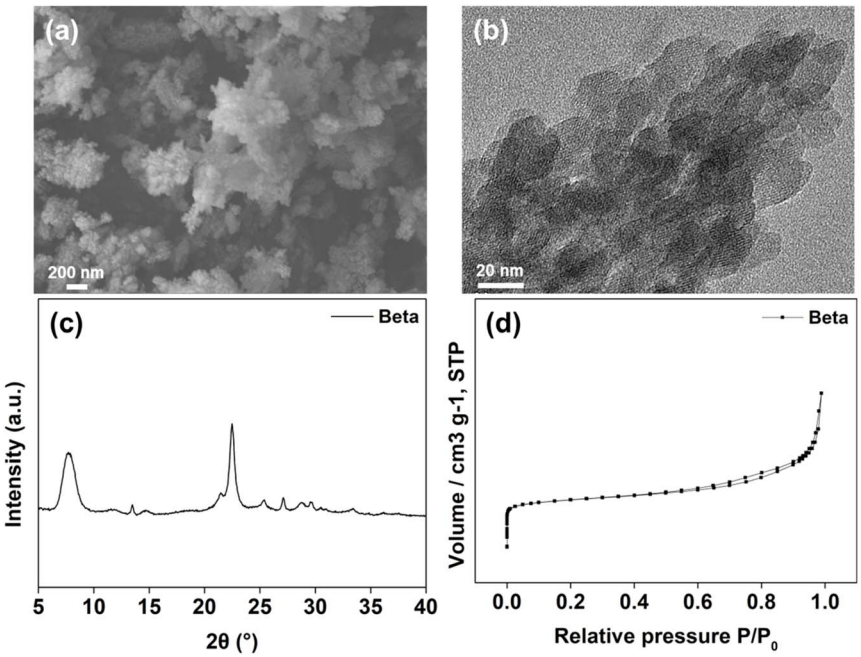

Fig. 2 (a) SEM image, (b) TEM image, (c) XRD patterns and (d) N_2 sorption isotherms of beta zeolite.

Open Access Article. Published on 03 December 2024. Downloaded on 2/11/2026 7:43:27 PM.
This article is licensed under a Creative Commons Attribution-NonCommercial 3.0 Unported Licence.

Table 1 Texture properties of different samples

Samples	Si/Al[a]	S_{BET}[b] ($m^2\ g^{-1}$)	S_{micro}[c] ($m^2\ g^{-1}$)	S_{meso}[d] ($m^2\ g^{-1}$)	V_{micro}[e] ($cm^3\ g^{-1}$)	V_{meso}[f] ($cm^3\ g^{-1}$)	V_{total}[g] ($cm^3\ g^{-1}$)
B-fresh	15.46	627	420	207	0.17	0.78	0.95
B-SN	—	500	357	143	0.14	0.53	0.67
B-coke	—	86	0	86	0.00	0.55	0.55
Coke-burning	18.68	600.93	415.58	185.35	0.16	0.76	0.92

[a] The Si/Al ratio was measured using ICP-AES. [b] The total surface area was calculated *via* the BET method. [c] The micropore surface area was calculated using the *t*-plot method. [d] The mesopore surface area was calculated through the subtraction of S_{BET} by S_{micro}. [e] The micropore volume calculated using the *t*-plot method. [f] The mesopore volume was calculated through the subtraction of V_{total} by V_{micro}. [g] The total pore volume was obtained at a relative pressure of 0.98.

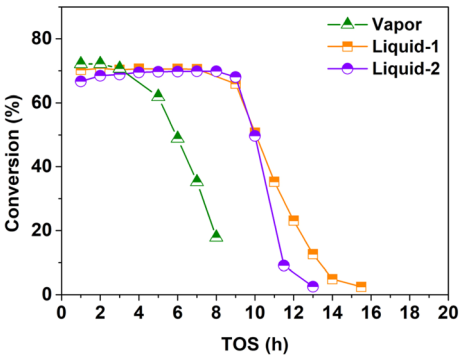

Fig. 3 Effect of the reaction phase on catalytic performance. Reaction conditions: (a) liquid phase-1, 260 °C, 4.0 MPa, 13 wt% 1-MN/benzene, and 5 h^{-1}; (b) liquid phase-2, 260 °C, 4.0 MPa, 6.5 wt% 1-MN/benzene, and 10 h^{-1}; (c) vapor phase, 260 °C, 0.1 MPa, 13 wt% 1-MN/benzene, 5 h^{-1}, and 20 ml per min N_2.

and concentration of 1-MN on the catalytic performance are shown in Fig. 4. As can be seen, the lifetime first increased and then decreased gradually with increasing temperature. In fact, for the initial 5–10 h, similar catalytic performances were obtained at different temperatures. However, it is difficult to obtain the optimal reaction conditions in a large gradient. Therefore, we conducted a study on the effect of temperature in a smaller gradient and a longer reaction duration. The catalyst exhibited optimum performance at 252 °C. For the effect of WHSV, the lifetime increased gradually as WHSV decreased. Similarly, decreasing the concentration of 1-MN can also increase the lifetime. However, the WHSV and concentration of 1-MN should not be too low for practical production, and the operation cost should also be considered.

3.3 Deactivation and regeneration

Generally speaking, the deactivation of zeolite-catalyzed reactions is usually caused by coke.[11–14,53–55] However, the active sites

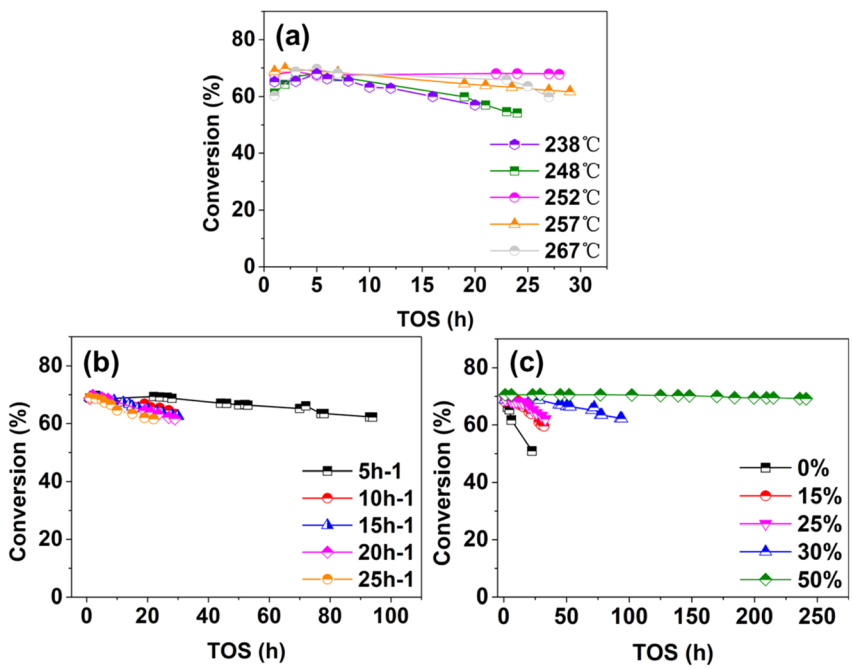

Fig. 4 Optimization process of reaction conditions. (a) Effect of temperature. Reaction conditions: 4.0 MPa, 6.5 wt% 1-MN, and 10 h^{-1}. (b) Effect of WHSV. Reaction conditions: 252 °C, 4.0 MPa, and 6.5 wt% 1-MN. (c) Effect of the concentration of benzene. Reaction conditions: 252 °C, 4.0 MPa, and 10 h^{-1}.

© 2024 The Author(s). Published by the Royal Society of Chemistry

Open Access Article. Published on 03 December 2024. Downloaded on 2/11/2026 7:43:27 PM.
This article is licensed under a Creative Commons Attribution-NonCommercial 3.0 Unported Licence.

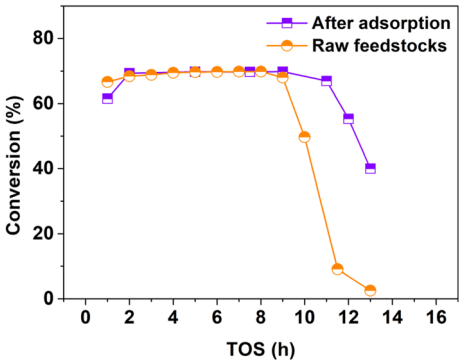

Fig. 5 Comparison of the catalytic performance with different amounts of sulfide and nitride. Reaction conditions: 260 °C, 4.0 MPa, 6.5 wt% 1-MN, and 4 h^{-1}.

can also be poisoned by some molecules. For example, Han *et al.* found that there exists competitive adsorption between reactants and the oxygenated organic compounds for the MWW zeolite-catalyzed alkylation of benzene with 1-dodecene.[56] A similar phenomenon has also been reported for the metal-catalyzed reactions.[57–59] For the zeolite-catalyzed isomerization of 1-MN investigated in this work, the feedstocks are usually contaminated with some sulfide and nitride. However, the effect of these sulfide and nitride contaminants has rarely been reported. Therefore, the catalytic performances using feedstocks with different amounts of sulfide and nitride will be discussed as follows.

The preparation of feedstocks with different amounts of sulfide and nitride is elucidated in the ESI (see S1).† It should be noted that, owing to the limitation of this method, it is difficult to decrease the amount of sulfide. Therefore, the following discussions are mainly focused on the effect of nitride. On the other hand, the effect of sulfide on the reaction is limited, which was proved by DFT calculations (see Fig. 7 and Table 2).

Firstly, 1-MN with different amounts of nitride was fed into the reactor. As can be seen from Fig. 5, the lifetime was only 9 h when the amount of nitride was 1188.28 ppm. As the amount of nitride was decreased to 824.57 ppm, the lifetime was extended to 11 h correspondingly. Therefore, it can be inferred that the nitrides contaminated in the feedstocks are detrimental to the reactions.

The texture properties of different samples are shown in Fig. 6a and Table 1. As can be seen, a slight decrease of the surface area occurred for B-SN. However, the surface area of B-coke decreased in a large extent, especially for the micropores. Therefore, it can be inferred that the organics deposed on the zeolite surface are different when different feedstocks are utilized. The TG curves of different samples are shown in Fig. 6b. As can be seen, B-coke exhibits 33.39% weight loss. However, only 16.53% weight loss occurred for B-SN, indicating that less organics were deposed on the zeolite surface. The rapid decrease of B-coke was mainly due to the accumulation of large size molecules on the zeolite surface, which would be calcinated with increasing temperature. However, the acid sites of B-SN were mainly covered by nitrides, therefore a slower decreasing trend was observed. This conclusion agrees well with the discussion above.

Furthermore, DFT calculations were conducted to gain deeper insight into the deactivation mechanism. Firstly, we selected quinoline, indole, aniline, thiophene and 1-benzothiophene as the model sulfide and nitride to investigate their effects. It has been reported that the orientations of the guest species in the zeolite channels greatly affect their thermostability.[60–62] Accordingly, multi-geometry searching for the adsorption structures was firstly conducted, and the most stable configuration was considered in the text (see Fig. 7). The adsorption energies of different molecules are shown in Table 2. As can be seen, the adsorption energies of all the nitride are larger than that of 1-MN and 2-MN. On the other hand, the variation of the O–H bond length can also reflect the proximity of different molecules on the acidic sites. As can be seen from Table 2, the corresponding variations of the O–H bond length are also larger for nitride, indicating their strongly competitive adsorption. However, the effect of sulfide is less than that of nitride, whether for the adsorption or variation of the O–H bond length. Based on the discussion above, it can be concluded that the deactivation when feeding with nitride and sulfide should be mainly attributed to the higher proximity of nitride on the acid sites than that of 1-MN and 2-MN.

For the microporous characteristics of zeolites, deactivation by coke is usually unavoidable in the catalytic processes.[11–14,53–55] Generally, the deactivated zeolites can be regenerated by extraction with organic solvents or coke-burning.[11,12,63,64] For the reactions occurring in a fixed bed reactor, extraction with

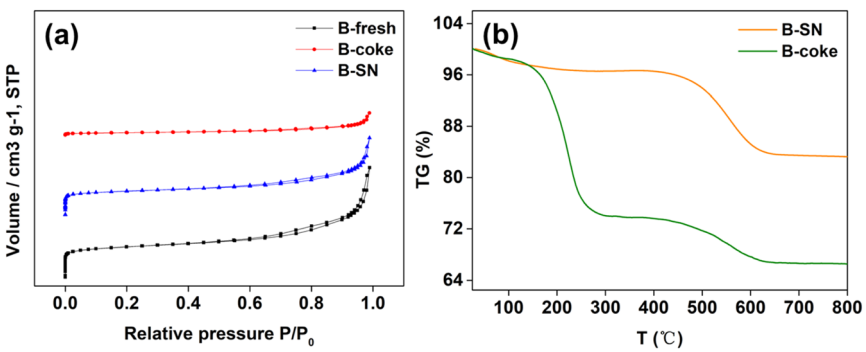

Fig. 6 (a) N_2 sorption isotherms and (b) TG curves of different samples.

Open Access Article. Published on 03 December 2024. Downloaded on 2/11/2026 7:43:27 PM.
This article is licensed under a Creative Commons Attribution-NonCommercial 3.0 Unported Licence.

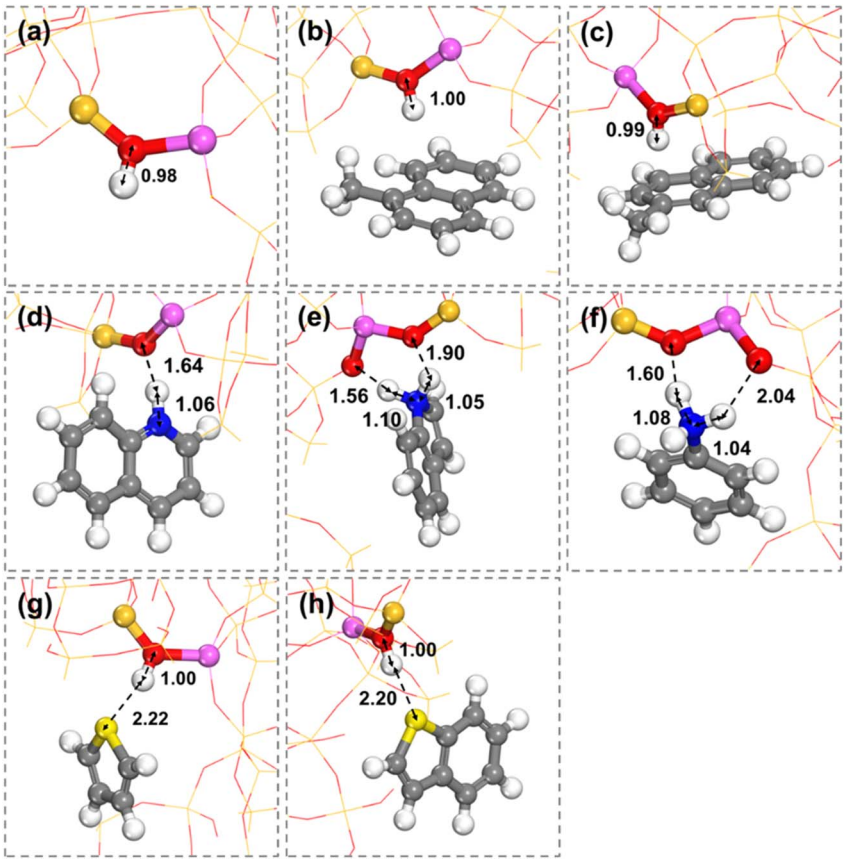

Fig. 7 Local geometry structures of the acid sites adsorbed different molecules: (a) initial state, (b) 1-MN, (c) 2-MN, (d) quinoline, (e) indole, (f) aniline, (g) thiophene, and (h) 1-benzothiophene. All distances are in Å.

Table 2 Effect of different molecules on the adsorption energy and variation of the O–H bond length

				Nitride			Sulfide	
	Initial state	1-MN	2-MN	Quinoline	Indole	Aniline	Thiophene	1-Benzothiophene
Adsorption energy (eV)	—	1.48	1.40	2.49	1.51	2.05	0.80	1.16
Bond length of H–O– (Å)	0.98	1.00	0.99	1.64	1.90	1.60	1.00	1.00

organic solvents is usually the primary choice to regenerate the deactivated catalysts.[12] Herein, we first attempt to recover the activity of the deactivated catalysts by extraction with hot benzene at 250 °C. As can be seen from Fig. 8, the activity cannot be recovered by extraction with benzene, indicating the firm adsorption of nitride and sulfide. Therefore, we attempted to regenerate the catalyst by coke-burning. Fortunately, the activity and lifetime can be effectively recovered by coke-burning at 475 °C to 550 °C (see Fig. 8).

The XRD patterns of the calcinated beta are shown in Fig. 9a. As can be seen, the diffraction intensity of the calcinated zeolite is comparable with that of the fresh beta. Additionally, the surface areas are preserved well (see Table 1), indicating that the framework was effectively preserved during the coke-burning. The ^{27}Al NMR spectra of beta zeolite are shown in Fig. 9b. It can be seen that Al was extracted from the framework after calcination. The NH_3-TPD curves are shown in Fig. 9c. As can be

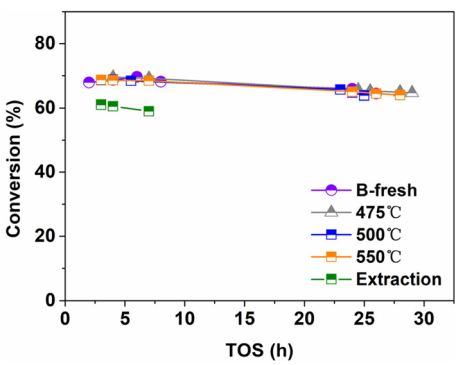

Fig. 8 Regeneration by extraction with benzene and coke-burning. Reaction conditions: 260 °C, 4.0 MPa, 6.5 wt% 1-MN, and 10 h^{-1}. Extraction conditions: 100 °C, 4.2 MPa, 15/1, and 16 h^{-1}. Coke-burning conditions: 475 °C/500 °C/550 °C for 5 h in 100 ml per min air flow.

© 2024 The Author(s). Published by the Royal Society of Chemistry

Open Access Article. Published on 03 December 2024. Downloaded on 2/11/2026 7:43:27 PM.
This article is licensed under a Creative Commons Attribution-NonCommercial 3.0 Unported Licence.

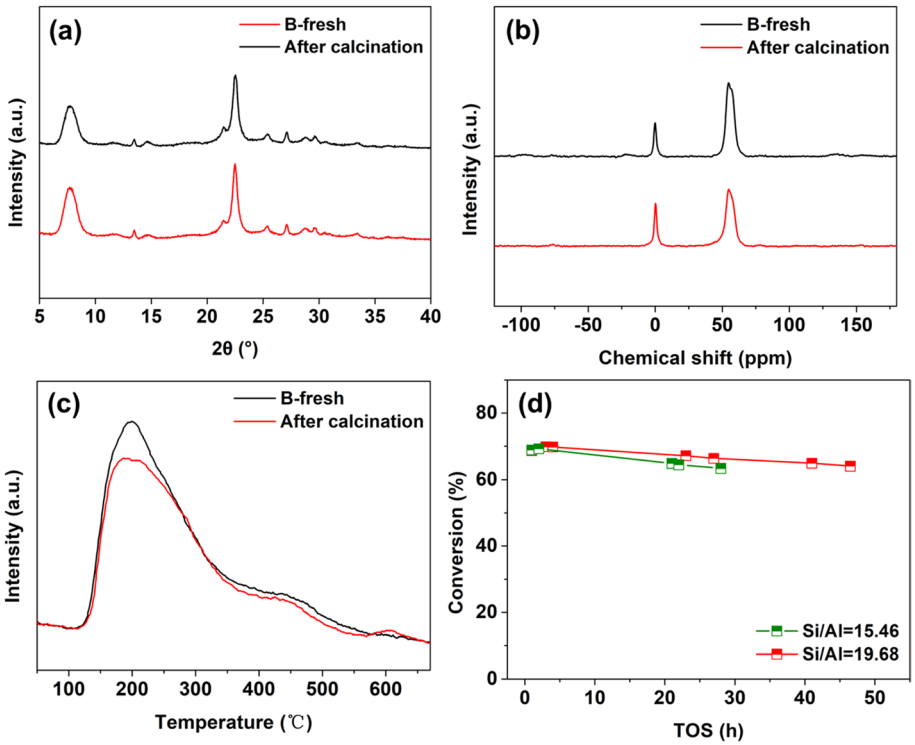

Fig. 9 (a–c) Comparison of the texture properties of fresh and calcined zeolites. (d) Comparison of the catalytic performance using zeolite with different Si/Al ratios.

seen, a slight decrease of the acid amount occurred during the calcination, which was consistent with the ^{27}Al NMR spectra. For the zeolite-catalyzed isomerization of 1-MN in this work, the activity is mainly contributed by acid sites. However, the catalytic performance of the calcinated beta is comparable with that of the fresh one, indicating that the catalytic performance is not positively correlated with the acid amount. Furthermore, we conducted the isomerization of 1-MN over the beta zeolite with different Si/Al. As can be seen from Fig. 9d, increasing Si/Al is beneficial to the catalytic performance, which agrees well with the discussion above.

In fact, the relationship between the acid properties and catalytic performance can be found in a variety of previous works from the literature.[39,65–68] However, the relationship differs for different reactions. There exists a suitable acid amount or distribution for some determined reactions. In terms of the accurate relationship and corresponding explanations about the acid properties and catalytic performance of the 1-MN isomerization, we assume that the main reaction and side reactions are influenced by the acid properties simultaneously. And there exists a balance between them. An accurate relationship and explanation should be investigated along the optimizing process of synthesizing a large amount of beta zeolite, and this work is also the required step for the industrial production.

4. Conclusion

In summary, the reaction processes of the beta-catalyzed isomerization of 1-MN were comprehensively investigated. The deactivation mechanism was elucidated in combination with characterization techniques and DFT calculations. It was revealed that the nitride in the feedstocks is detrimental to the reaction. The deactivation using the nitride contaminated feedstocks mainly caused the firm adsorption of nitride on the acid site. Furthermore, the deactivated catalyst is difficult to recover by extraction with hot benzene. Fortunately, the activity can be effectively regenerated by coke-burning. Theses experimental and theoretical insights can not only enable us to understand the deactivation mechanism in more detail, but they can also provide significant guidance for industrial production.

Data availability

Data for this article, including characterization, evaluation, and DFT calculations, are available at **https://pan.baidu.com/s/1NzSaoahfj3n0kv0e0RjJlA?pwd=7npr**.

Conflicts of interest

The authors declare that they have no known competing financial interests or personal relationships that could have appeared to influence the work reported in this paper.

Acknowledgements

We acknowledge our group members for the discussion of the results.

Open Access Article. Published on 03 December 2024. Downloaded on 2/11/2026 7:43:27 PM. This article is licensed under a Creative Commons Attribution-NonCommercial 3.0 Unported Licence.

References

1 J. Li, Q. Gong, H. Lian, L. Ding, Z. Hu and Z. Zhu, Transalkylation of C10 aromatics with 2-methylnaphthalene for 2,6-dimethylnaphthalene synthesis: high-efficiently shape-selective & synergistic catalysis over a multifunctional SiO2-Mo-HBeta catalyst, *J. Catal.*, 2019, **378**, 144–152.

2 Q. Liu, L. Jiang, H. Shi, D. Zhao, L. Zhou, R. Zhang, R. Ye, D. Wang and G. Feng, HBEA/MTW composite molecular sieves with shape-selectively catalyzed alkylation of 2-methylnaphthalene with methanol for the synthesis of 2,6-dimethylnaphthalene, *Mol. Catal.*, 2023, **549**, 113472.

3 W. Xiang, W. Wang, C. Hou, C. Fan, T. Lei, J. Li and M. Ge, Secondary organic aerosols from oxidation of 1-methylnaphthalene: yield, composition, and volatility, *Sci. Total Environ.*, 2024, 170379.

4 X. Ma, S. Shi, Q. Xu, L. Xu and G. Liu, Selective hydrogenation of 2-methylnaphthalene by heterostructured Ni-NiO-based catalysts for 6-methyl-1,2,3,4-tetrahydronaphthalene, *Mol. Catal.*, 2022, **529**, 112537.

5 R. Ye, Q. Liu, Z. Wen, L. Jiang, C. Jin, B. Gao, B. Zhang, R. Zhang, Y. Qin and G. Feng, Shape-selective catalysts of Mg2+ ion exchange modified SAPO-11 molecular sieves for alkylation of 2-methylnaphthalene, *Microporous Mesoporous Mater.*, 2022, **346**, 112291.

6 H. Sun, S. Shi and Z. Gu, Isomerization of alkyl naphthalene and refining of 2-methylnaphthalene, *Chin. J. Chem. Eng.*, 2017, **25**, 149–152.

7 L. D. Lillwitz, Production of dimethyl-2,6-naphthalenedicarboxylate: precursor to polyethylene naphthalate, *Appl. Catal., A*, 2001, **221**, 337–358.

8 S.-B. Pu and T. Inui, Synthesis of 2,6-dimethylnaphthalene by methylation of methylnaphthalene on various medium and large-pore zeolite catalysts, *Appl. Catal., A*, 1996, **146**, 305–316.

9 A. Arkhireyeva and S. Hashemi, Fracture behaviour of polyethylene naphthalate (PEN), *Polymer*, 2002, **43**, 289–300.

10 H.-t. Li, L.-y. Sheng, J.-l. Zhan, W.-x. Fang, Y. Liang and Y. Zhang, Comparative study on the catalytic performance of zeolite catalysts with different topologies in 1-methylnaphthalene isomerization-transalkylation coupling reaction, *J. Fuel Chem. Technol.*, 2021, **49**, 809–817.

11 N. Chaouati, A. Soualah, M. Chater, M. Tarighi and L. Pinard, Mechanisms of coke growth on mordenite zeolite, *J. Catal.*, 2016, **344**, 354–364.

12 M. Díaz, E. Epelde, J. Valecillos, S. Izaddoust, A. T. Aguayo and J. Bilbao, Coke deactivation and regeneration of HZSM-5 zeolite catalysts in the oligomerization of 1-butene, *Appl. Catal., B*, 2021, **291**, 120076.

13 S. Inagaki, S. Shinoda, Y. Kaneko, K. Takechi, R. Komatsu, Y. Tsuboi, H. Yamazaki, J. N. Kondo and Y. Kubota, Facile Fabrication of ZSM-5 Zeolite Catalyst with High Durability to Coke Formation during Catalytic Cracking of Paraffins, *ACS Catal.*, 2013, **3**, 74–78.

14 Z. Ma, X. Hou, B. Chen, L. Zhao, E. Yuan and T. Cui, Experiment and modeling of coke formation and catalyst deactivation in n-heptane catalytic cracking over HZSM-5 zeolites, *Chin. J. Chem. Eng.*, 2023, **55**, 165–172.

15 Z. Popova, M. Yankov, L. Dimitrov and I. Chervenkov, Isomerization and disproportionation of 1-methylnaphthalene on zeolites, *React. Kinet. Catal. Lett.*, 1994, **52**, 51–58.

16 J. Weitkamp and M. Neuber, Shape Selective Reactions of Alkylnaphthalenes in Zeolite Catalysts, in *Studies in Surface Science and Catalysis*, ed. T. lnui, S. Namba and T. Tatsumi, Elsevier, 1991, pp. 291–301.

17 H. Lee, J. Shin, K. Lee, J. C. Hyun, A. Mayoral, Y. K. Na and B. H. Suk, Synthesis of thermally stable SBT and SBS/SBT intergrowth zeolites, *Science*, 2021, **373**, 104–107.

18 S. Li, J. Li, M. Dong, S. Fan, T. Zhao, J. Wang and W. Fan, Strategies to control zeolite particle morphology, *Chem. Soc. Rev.*, 2019, **48**, 885–907.

19 N. Wang, Q. Sun, T. Zhang, A. Mayoral, L. Li, X. Zhou, J. Xu, P. Zhang and J. Yu, Impregnating Subnanometer Metallic Nanocatalysts into Self-Pillared Zeolite Nanosheets, *J. Am. Chem. Soc.*, 2021, **143**, 6905–6914.

20 M. Choi, K. Na, J. Kim, Y. Sakamoto, O. Terasaki and R. Ryoo, Stable single-unit-cell nanosheets of zeolite MFI as active and long-lived catalysts, *Nature*, 2009, **461**, 246–249.

21 Q. Zhang, J. Yu and A. Corma, Applications of Zeolites to C1 Chemistry: Recent Advances, Challenges, and Opportunities, *Adv. Mater.*, 2020, **32**, 2002927.

22 D. Xu, Y. Ma, Z. Jing, L. Han, B. Singh, J. Feng, X. Shen, F. Cao, P. Oleynikov, H. Sun, O. Terasaki and S. Che, π–π interaction of aromatic groups in amphiphilic molecules directing for single-crystalline mesostructured zeolite nanosheets, *Nat. Commun.*, 2014, **5**, 4262.

23 V. Valtchev and L. Tosheva, Porous Nanosized Particles: Preparation, Properties, and Applications, *Chem. Rev.*, 2013, **113**, 6734–6760.

24 S. Lin, Y. Zhi, W. Chen, H. Li, W. Zhang, C. Lou, X. Wu, S. Zeng, S. Xu, J. Xiao, A. Zheng, Y. Wei and Z. Liu, Molecular Routes of Dynamic Autocatalysis for Methanol-to-Hydrocarbons Reaction, *J. Am. Chem. Soc.*, 2021, **143**, 12038–12052.

25 H. Dai, Y. Shen, T. Yang, C. Lee, D. Fu, A. Agarwal, T. T. Le, M. Tsapatsis, J. C. Palmer, B. M. Weckhuysen, P. J. Dauenhauer, X. Zou and J. D. Rimer, Finned zeolite catalysts, *Nat. Mater.*, 2020, **19**, 1074–1080.

26 M. Khaleel, A. J. Wagner, K. A. Mkhoyan and M. Tsapatsis, On the Rotational Intergrowth of Hierarchical FAU/EMT Zeolites, *Angew. Chem., Int. Ed.*, 2014, **53**, 9456–9461.

27 J. Deng, X. Wang, Z. Wei, L. Wang, C. Wang and Z. Chen, A review of NOx and SOx emission reduction technologies for marine diesel engines and the potential evaluation of liquefied natural gas fuelled vessels, *Sci. Total Environ.*, 2021, **766**, 144319.

28 U. Asghar, S. Rafiq, A. Anwar, T. Iqbal, A. Ahmed, F. Jamil, M. S. Khurram, M. M. Akbar, A. Farooq, N. S. Shah and Y.-K. Park, Review on the progress in emission control

© 2024 The Author(s). Published by the Royal Society of Chemistry

Open Access Article. Published on 03 December 2024. Downloaded on 2/11/2026 7:43:27 PM. This article is licensed under a Creative Commons Attribution-NonCommercial 3.0 Unported Licence.

technologies for the abatement of CO2, SOx and NOx from fuel combustion, *J. Environ. Chem. Eng.*, 2021, **9**, 106064.
29 D. Kim, H. Ahn, W. Yang, K. Y. Huh and Y. Lee, Experimental analysis of CO/H2 syngas with NOx and SOx reactions in pressurized oxy-fuel combustion, *Energy*, 2021, **219**, 119550.
30 M. Mollo, A. Kolesnikov and S. Makgato, Simultaneous reduction of NOx emission and SOx emission aided by improved efficiency of a Once-Through Benson Type Coal Boiler, *Energy*, 2022, **248**, 123551.
31 M. Y. Mohammed, A. M. Ali and T. M. Albayati, Choline chloride-based deep eutectic solvents for ultrasonic-assisted oxidative desulfurization of actual heavy crude oil, *Chem. Eng. Res. Des.*, 2022, **182**, 659–666.
32 P. Naveen and M. D. Kumar, Desulfurization of sour crude oil using an invasive weed adsorbent: an efficient, eco-friendly, and ultra-low-cost option, *J. Indian Chem. Soc.*, 2022, **99**, 100305.
33 A. Solouki, S. A. Jaffer and J. Chaouki, Process development and techno-economic analysis of microwave-assisted demetallization and desulfurization of crude petroleum oil, *Energy Rep.*, 2022, **8**, 4373–4385.
34 J. P. Pietroski, J. R. White, R. D. DeLaune, J. J. Wang and S. K. Dodla, Fresh and weathered crude oil effects on potential denitrification rates of coastal marsh soil, *Chemosphere*, 2015, **134**, 120–126.
35 H. Ribeiro, A. P. Mucha, I. Azevedo, P. Salgado, C. Teixeira, C. M. R. Almeida, S. B. Joye and C. Magalhães, Differential effects of crude oil on denitrification and anammox, and the impact on N2O production, *Environ. Pollut.*, 2016, **216**, 391–399.
36 U. Agarwal, M. S. Rigutto, E. Zuidema, A. P. J. Jansen, A. Poursaeidesfahani, S. Sharma, D. Dubbeldam and T. J. H. Vlugt, Kinetics of zeolite-catalyzed heptane hydroisomerization and hydrocracking with CBMC-modeled adsorption terms: zeolite beta as a large pore base case, *J. Catal.*, 2022, **415**, 37–50.
37 T. Aumond, M. Esteves, Y. Pouilloux, R. Faccio and A. Sachse, Impact of the crystal size of beta zeolite on the structural quality of zeolite templated carbons, *Microporous Mesoporous Mater.*, 2022, **331**, 111644.
38 Z. Liu, H. Li, Y. Wang, Y. Wang, P. Peng and X. Liu, Seeds induced beta zeolite synthesis with low SDA for n-heptane catalytic cracking reaction, *Catal. Today*, 2022, **405–406**, 235–241.
39 R. Li, S. Xing, S. Zhang and M. Han, Effect of surface silicon modification of H-beta zeolites for alkylation of benzene with 1-dodecene, *RSC Adv.*, 2020, **10**, 10006–10016.
40 G. Kresse and J. Furthmüller, Efficiency of ab initio total energy calculations for metals and semiconductors using a plane-wave basis set, *Comput. Mater. Sci.*, 1996, **6**, 15–50.
41 G. Kresse and J. Hafner, Ab initio molecular-dynamics simulation of the liquid-metal-amorphous-semiconductor transition in germanium, *Phys. Rev. B:Condens. Matter Mater. Phys.*, 1994, **49**, 14251–14269.
42 S. Grimme, J. Antony, S. Ehrlich and H. Krieg, A Consistent and Accurate Ab Initio Parametrization of Density Functional Dispersion Correction (DFT-D) for the 94 Elements H-Pu, *J. Chem. Phys.*, 2010, **132**, 154104.
43 P. E. Blöchl, Projector augmented-wave method, *Phys. Rev. B:Condens. Matter Mater. Phys.*, 1994, **50**, 17953–17979.
44 G. Kresse and D. Joubert, From ultrasoft pseudopotentials to the projector augmented-wave method, *Phys. Rev. B:Condens. Matter Mater. Phys.*, 1999, **59**, 1758–1775.
45 H. J. Monkhorst and J. D. Pack, Special points for Brillouin-zone integrations, *Phys. Rev. B*, 1976, **13**, 5188–5192.
46 Structure Commision of the International Zeolite Association, **http://www.iza-structure.org/databases/**.
47 Y.-L. Wang, X.-X. Wang, Y.-A. Zhu, K.-K. Zhu, D. Chen and X.-G. Zhou, Shape selectivity in acidic zeolite catalyzed 2-pentene skeletal isomerization from first principles, *Catal. Today*, 2020, **347**, 115–123.
48 M. Boronat, A. Corma, M. Renz, G. Sastre and P. Viruela, A Multisite Molecular Mechanism for Baeyer-Villiger Oxidations on Solid Catalysts Using Environmentally Friendly H2O2 as Oxidant, *Chem.–Eur. J.*, 2005, **11**, 6905–6915.
49 H. Fujita, T. Kanougi and T. Atoguchi, Distribution of Brønsted acid sites on beta zeolite H-BEA: a periodic density functional theory calculation, *Appl. Catal., A*, 2006, **313**, 160–166.
50 A. Andersen, N. Govind and L. Subramanian, Theoretical study of the mechanism behind the para-selective nitration of toluene in zeolite H-beta, *Mol. Simul.*, 2008, **34**, 1025–1039.
51 Z. Popova, M. Yankov and L. Dimitrov, Methylation, Isomerization and Disproportionation of Naphthalene and Methylnaphthalenes on Zeolite Catalysts, in *Studies in Surface Science and Catalysis*, ed. J. Weitkamp, H. G. Karge, H. Pfeifer and W. Hölderich, Elsevier, 1994, pp. 1829–1835.
52 M. A. Camblor, A. Corma and S. Valencia, Characterization of nanocrystalline zeolite beta, *Microporous Mesoporous Mater.*, 1998, **25**, 59–74.
53 X.-Y. Ren, J.-P. Cao, S.-X. Zhao, X.-Y. Zhao, X.-B. Feng, T.-L. Liu, Y. Li, J. Zhang and X.-Y. Wei, Insights into coke location of catalyst deactivation during in situ catalytic reforming of lignite pyrolysis volatiles over cobalt-modified zeolites, *Appl. Catal., A*, 2021, **613**, 118018.
54 D. Rojo-Gama, M. Nielsen, D. S. Wragg, M. Dyballa, J. Holzinger, H. Falsig, L. F. Lundegaard, P. Beato, R. Y. Brogaard, K. P. Lillerud, U. Olsbye and S. Svelle, A Straightforward Descriptor for the Deactivation of Zeolite Catalyst H-ZSM-5, *ACS Catal.*, 2017, **7**, 8235–8246.
55 A. G. Gayubo, A. Alonso, B. Valle, A. T. Aguayo and J. Bilbao, Deactivation kinetics of a HZSM-5 zeolite catalyst treated with alkali for the transformation of bio-ethanol into hydrocarbons, *AIChE J.*, 2012, **58**, 526–537.
56 S. Xing, Y. Cui, T. Wang, J. He and M. Han, Elucidating the effect of oxides on the zeolite catalyzed alkylation of benzene with 1-dodecene, *Chin. J. Chem. Eng.*, 2023, **56**, 126–135.
57 S. C. McGuire, N. R. Hurley, M. G. Gallagher, L. Zhang, A. I. Frenkel and S. S. Wong, Assessing the roles of synthesis method and chemical composition in determining structure–property correlations in alloyed,

Open Access Article. Published on 03 December 2024. Downloaded on 2/11/2026 7:43:27 PM.
This article is licensed under a Creative Commons Attribution-NonCommercial 3.0 Unported Licence.

ultrathin nanowire motifs for the methanol oxidation reaction, *Energy Adv.*, 2024, **3**, 163–176.

58 Z. Cheng, J.-H. Wang, Y. Choi, L. Yang, M. C. Lin and M. Liu, From Ni-YSZ to sulfur-tolerant anode materials for SOFCs: electrochemical behavior, in situ characterization, modeling, and future perspectives, *Energy Environ. Sci.*, 2011, **4**, 4380–4409.

59 W. Luo, Y. Jiang, M. Wang, D. Lu, X. Sun and H. Zhang, Design strategies of Pt-based electrocatalysts and tolerance strategies in fuel cells: a review, *RSC Adv.*, 2023, **13**, 4803–4822.

60 C.-M. Wang, Y.-D. Wang, Y.-J. Du, G. Yang and Z.-K. Xie, Computational insights into the reaction mechanism of methanol-to-olefins conversion in H-ZSM-5: nature of hydrocarbon pool, *Catal. Sci. Technol.*, 2016, **6**, 3279–3288.

61 D. Wang, C.-M. Wang, G. Yang, Y.-J. Du and W.-M. Yang, First-principles kinetic study on benzene alkylation with ethanol vs. ethylene in H-ZSM-5, *J. Catal.*, 2019, **374**, 1–11.

62 S. Xing, K. Liu, T. Wang, R. Zhang and M. Han, Elucidation of the mechanism and structure–reactivity relationship in zeolite catalyzed alkylation of benzene with propylene, *Catal. Sci. Technol.*, 2021, **11**, 2792–2804.

63 Y. Nakasaka, T. Tago, H. Konno, A. Okabe and T. Masuda, Kinetic study for burning regeneration of coked MFI-type zeolite and numerical modeling for regeneration process in a fixed-bed reactor, *Chem. Eng. J.*, 2012, **207–208**, 368–376.

64 Y. Song, S. Liu, Q. Wang, L. Xu and Y. Zhai, Coke burning behavior of a catalyst of ZSM-5/ZSM-11 co-crystallized zeolite in the alkylation of benzene with FCC off-gas to ethylbenzene, *Fuel Process. Technol.*, 2006, **87**, 297–302.

65 S. Xing, R. Zhang and M. Han, Structure/acid-reactivity relationship of the zeolite catalyzed alkylation of benzene with 1-dodecene by constructing micro-meso composites, *Mol. Catal.*, 2022, **531**, 112703.

66 S. Kokuryo, K. Tamura, S. Tsubota, K. Miyake, Y. Uchida, A. Mizusawa, T. Kubo and N. Nishiyama, Selective recovery of light olefins from polyolefin catalyzed by Lewis acidic Sn-Beta zeolites without Brønsted acidity, *Catal. Sci. Technol.*, 2024, **14**, 3589–3595, DOI: **10.1039/d4cy00317a**.

67 L. Wang, L. Fan, Y. Wang, Q. Chen, Y. Zhu and Y. Yi, Tuning selectivity of acetic acid and alcohols by Brønsted and Lewis acid sites in plasma-catalytic CH4/CO2 conversion over zeolites, *Appl. Catal., B*, 2024, **350**, 123938.

68 Y. Chen, T. Lu, X. Yang and L. Zhou, Regulation of acid/basic properties of Zr-beta zeolite for efficient conversion of furfural to furfuryl alcohol, *Mol. Catal.*, 2024, **559**, 114093.

© 2024 The Author(s). Published by the Royal Society of Chemistry